Long-lived oscillatory incoherent electron dynamics in molecules: *trans*-polyacetylene oligomers

Ignacio Franco[1,4]**, Angel Rubio**[1,2] **and Paul Brumer**[3]

[1] Theory Department, Fritz Haber Institute of the Max Planck Society, Faradayweg 4-6, D-14195 Berlin, Germany
[2] Nano-Bio Spectroscopy group, Departamento de Física de Materiales, Universidad del País Vasco, Centro de Física de Materiales CSIC-UPV/EHU-MPC and DIPC, Avenida Tolosa 72, E-20018 San Sebastián, Spain
[3] Chemical Physics Theory Group and Department of Chemistry, University of Toronto, Toronto, ON M5S 3H6, Canada
E-mail: franco@fhi-berlin.mpg.de

Abstract. We identify an intriguing feature of the electron–vibrational dynamics of molecular systems via a computational examination of *trans*-polyacetylene oligomers. Here, via the vibronic interactions, the decay of an electron in the conduction band resonantly excites an electron in the valence band, and vice versa, leading to oscillatory exchange of electronic population between two distinct electronic states that lives for up to tens of picoseconds. The oscillatory structure is reminiscent of beating patterns between quantum states and is strongly suggestive of the presence of long-lived molecular electronic coherence. Significantly, however, a detailed analysis of the electronic coherence properties shows that the oscillatory structure arises from a purely incoherent process. These results were obtained by propagating the coupled dynamics of electronic and vibrational degrees of freedom in a mixed quantum-classical study of the Su–Schrieffer–Heeger Hamiltonian for polyacetylene. The incoherent process is shown to occur between degenerate electronic states with distinct

[4] Author to whom any correspondence should be addressed.

electronic configurations that are indirectly coupled via a third auxiliary state by vibronic interactions. A discussion of how to construct electronic superposition states in molecules that are truly robust to decoherence is also presented.

S Online supplementary data available from stacks.iop.org/NJP/15/043004/mmedia

Contents

1. Introduction

A characteristic feature of molecular systems is that they exhibit strong electron–vibrational interactions. Such vibronic couplings [1, 2] are an essential component of the photophysics of molecules, leading to vibrations upon electronic excitation [3], spectral line broadenings, non-radiative transitions [4–7], electronic relaxation [8] and decoherence [9–14].

In this paper, we identify an intriguing and novel feature of the electron–vibrational dynamics of *trans*-polyacetylene (PA) in which, via the vibronic interactions, the decay of an electron in the conduction band leads to resonant excitation of an electron in the valence band. The converse process (the decay of an electron in the valence band to a further inner state leading to excitation of an electron in the conduction band) also takes place and brings the system back to its original state. The result is long-lived oscillatory electron dynamics. Throughout we refer to this phenomenon as vibronically induced resonant electronic population transfer (VIBRET).

As a model of *trans*-PA, we employ the Su–Schrieffer–Heeger (SSH) Hamiltonian [15], a tight-binding model for PA with strong electron–vibrational interactions. The SSH Hamiltonian is often used to study the static and dynamic features introduced by strong electron–ion couplings in molecular systems [12, 16, 17]. It has been shown to be successful in capturing the basic electronic structure of PA, its photoinduced vibronic dynamics and the rich photophysics of polarons, breathers and kinks [3, 12, 18, 19]. The vibronic dynamics of SSH chains is followed by explicitly propagating the coupled dynamics of electronic and vibrational degrees of freedom in an Ehrenfest mixed quantum–classical approximation [12, 20–22], where the nuclei are treated classically and the electrons quantum mechanically. Effects of nuclear fluctuations and decoherence are captured by propagating an ensemble of trajectories with initial conditions obtained by sampling the ground-state nuclear Wigner phase-space distribution [23].

Below we show that for a specific class of initial states this model of the vibronic evolution leads to VIBRET in SSH chains that, depending on system size, can live for up

to tens of picoseconds. VIBRET is seen to arise between degenerate electronic states with distinct electronic configurations that are indirectly coupled via a third auxiliary state by the electron–vibration interactions in the system. Given this identified level structure, we investigate the effect of changing system size and the nature of the initial state on the dynamics.

A striking feature of VIBRET is that it leads to population oscillations among the relevant levels that are analogous to those observed in beatings that result from coherent superposition states. As such, these oscillations seem to indicate that underlying this dynamics is an electronic superposition state that can live for picoseconds, a timescale that is very long for electronic coherences [9, 11, 14, 24]. The question of whether the observed behavior is, in fact, due to a long-lived electronic coherence is particularly relevant because of spectroscopic observations in photosynthetic systems that suggest that unusually long-lived electronic coherences are possible in the Fenna–Matthew–Olson and related complexes [25–27], with timescales exceeding 400–600 fs. Such long-lived electronic coherences have also been noted in intrachain energy migration in conjugated polymers [28]. Hence, if the SSH model can sustain long-lived coherences even in the presence of strong vibronic couplings, an analysis of the coherence properties of the model may well shed light on this topical problem [29–42].

We have divided this analysis into three main components. In section 3.1, we discuss the essential phenomenology of VIBRET and clarify the basic structure behind the population oscillations. In section 3.2, we characterize the coherence properties of VIBRET by introducing reduced measures of the purity that are apt for many-particle systems. *Using these purity measures we show that, contrary to intuition, the long-lived oscillations observed during VIBRET are the result of an incoherent process.* Finally, in section 3.3, we demonstrate how to construct electronic superpositions in vibronic systems that are truly robust to decoherence. This set of results is expected to have implications in our understanding of vibronic and coherent-like phenomena in molecules, macromolecules and bulk materials.

2. Model and methods

In the SSH model, the PA is described as a tight-binding chain, where each site represents a CH unit, in which the π-electrons are coupled to distortions in the oligomer backbone by a parameterized electron–vibrational interaction. For an N-membered oligomer, the SSH Hamiltonian reads [15]

$$H_{\text{SSH}} = H_{\text{e}} + H_{\text{ph}}, \tag{1a}$$

where

$$H_{\text{e}} = \sum_{n=1,\sigma\pm1}^{N-1} [-t_0 + \alpha(u_{n+1} - u_n)](c_{n+1,\sigma}^{\dagger} c_{n,\sigma} + c_{n,\sigma}^{\dagger} c_{n+1,\sigma}) \tag{1b}$$

$$H_{\text{ph}} = \sum_{n=1}^{N} \frac{p_n^2}{2M} + \frac{K}{2} \sum_{n=1}^{N-1} (u_{n+1} - u_n)^2 \tag{1c}$$

are, respectively, the electronic (H_{e}) and nuclear (H_{ph}) parts of the Hamiltonian. Here u_n denotes the displacement of the nth CH site from the perfectly periodic position $x = na$ with a the lattice constant of the chain. M is the mass of the CH group, p_n is the momentum conjugate to u_n and K is an effective spring constant. The operator $c_{n,\sigma}^{\dagger}$ (or $c_{n,\sigma}$) creates (or annihilates) a fermion

on site n with spin σ and satisfies the usual fermionic anticommutation relations. The electronic component of the Hamiltonian consists of a term describing the hopping of π electrons along the chain with hopping integral t_0 and an electron–ion interaction term with coupling constant α. The quantity α couples the electronic states to the molecular geometry and constitutes a first-order correction to the hopping integral that depends on the nuclear geometry. Throughout this work, we assume neutral chains with clamped ends and use the standard set of SSH parameters for PA [15]: $t_0 = 2.5\,\mathrm{eV}$, $\alpha = 4.1\,\mathrm{eV\,\mathring{A}}$, $K = 21\,\mathrm{eV\,\mathring{A}^{-2}}$, $M = 1349.14\,\mathrm{eV\,fs^2\,\mathring{A}^{-2}}$ and $a = 1.22\,\mathring{A}$. While it is possible to supplement the model with on-site electron–electron interaction terms, for the discussion below these terms are not fundamental and do not change the main findings. We therefore focus on the usual case of non-interacting electrons coupled to phonons.

The method employed to propagate the electron–vibrational dynamics of SSH chains has been described in detail previously [12, 14]. Briefly, the dynamics is followed in the Ehrenfest approximation [20], where the nuclei move classically on a mean-field potential energy surface with forces given by

$$\dot{p}_n = -\langle \varphi(t) | \frac{\partial H_{SSH}}{\partial u_n} | \varphi(t) \rangle. \tag{2}$$

In turn, the antisymmetrized many-electron wavefunction $|\varphi(t)\rangle$ satisfies the time-dependent Schrödinger equation

$$i\hbar \frac{\partial}{\partial t} |\varphi(t)\rangle = H_e[\boldsymbol{u}(t)] |\varphi(t)\rangle, \tag{3}$$

where $\boldsymbol{u} \equiv (u_1, u_2, \ldots, u_N)$. Decoherence effects are incorporated by propagating an ensemble of quantum-classical trajectories with initial conditions selected by importance sampling of the ground-state nuclear Wigner distribution function [12, 23] of the oligomer obtained in the harmonic approximation. In this way, the dynamics reflects the initial nuclear quantum distribution and is subject to the level broadening and internal relaxation mechanism induced by the vibronic couplings. The results shown here correspond to averages over 10 000 trajectories, providing statistically converged results.

In its minimum energy conformation, the SSH Hamiltonian yields a chain with a perfect alternation of double and single bonds. Its electronic structure is composed of $N/2$ 'valence band' orbitals with negative energies and $N/2$ 'conduction band' orbitals with positive energies that in the long-chain limit are separated by an energy gap of 1.3 eV. The single-particle spectrum depends on the nuclear geometry and changes during the electron–vibrational dynamics. However, because of the electron–hole symmetry in the Hamiltonian, the orbital energies are always such that for each orbital in the valence band of energy $-\epsilon_i$ there is an orbital in the conduction band of energy ϵ_i.

3. Results and discussion

3.1. Vibronically induced resonant electronic population transfer (VIBRET)

3.1.1. Basic phenomenology. We begin by describing the basic phenomenology behind VIBRET. For this, consider the dynamics of an oligomer initially prepared in a separable superposition state of the form

$$|\Omega\rangle = (\, b_0|\Phi_0\rangle + b_1|\Phi_1\rangle \,) \otimes |\chi_0\rangle, \tag{4}$$
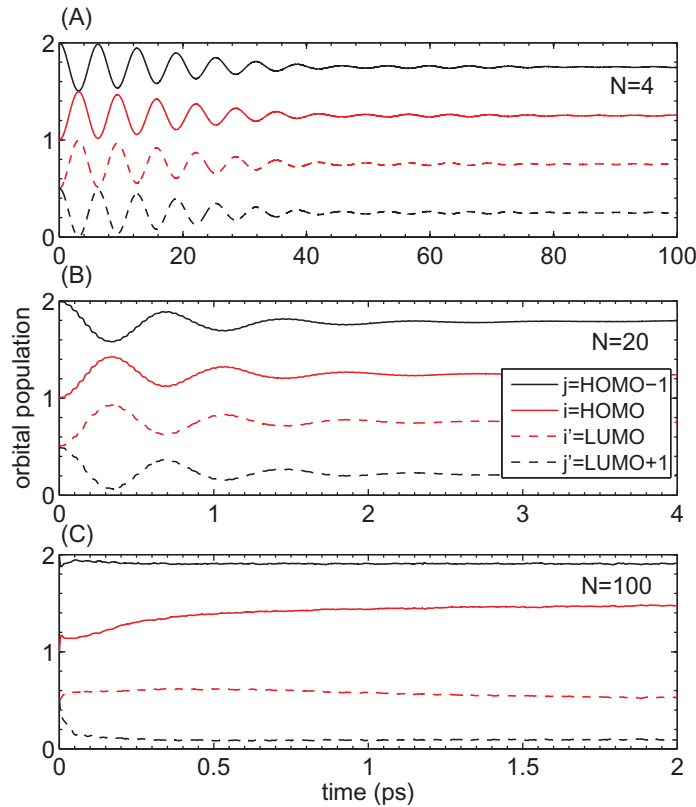
Figure 1. VIBRET in SSH chains with 4, 20 and 100 sites initially prepared in the superposition defined by equations (4) and (5), with $b_0 = b_1$. The figure shows the population of the orbitals involved during the complex vibronic evolution. Note the electronic population exchange among levels for $N = 4$ and 20.

where $|\chi_0\rangle$ is the initial nuclear state that, for definitiveness, we take to be the ground nuclear state of the ground electronic surface. As a first example, consider $b_0 = b_1$ and $|\Phi_0\rangle$ and $|\Phi_1\rangle$ to be the states obtained by HOMO→LUMO and HOMO→LUMO+1 transitions from the ground state in a given spin channel. That is,

$$|\Phi_0\rangle = c^{\dagger}_{\text{LUMO},\sigma} c_{\text{HOMO},\sigma} |\varphi_0\rangle,$$
$$|\Phi_1\rangle = c^{\dagger}_{\text{LUMO+1},\sigma} c_{\text{HOMO},\sigma} |\varphi_0\rangle, \tag{5}$$

where $|\varphi_0\rangle$ is the ground electronic state. Because of the electron–hole symmetry in the SSH approach, state $|\Phi_1\rangle$ is degenerate with the state

$$|\Phi_2\rangle = c^{\dagger}_{\text{LUMO},\sigma} c_{\text{HOMO}-1,\sigma} |\varphi_0\rangle. \tag{6}$$

States $|\Phi_1\rangle$ and $|\Phi_2\rangle$ have distinct electronic configuration and are thus orthonormal.

Figure 1 shows the population dynamics in the four relevant orbitals (HOMO $-$ 1, HOMO, LUMO, LUMO+1) involved during the dynamics for chains of different size ($N = 4$, 20 and 100). Focus first on $N = 4$ (figure 1(A)) where the vibronic dynamics shows a remarkable long-lived population transfer between levels that survive for tens of picoseconds. Such population exchange is what we refer to as VIBRET. An analysis of the orbital dynamics leads to the following interpretation of the observed behavior (a schematic diagram of the population
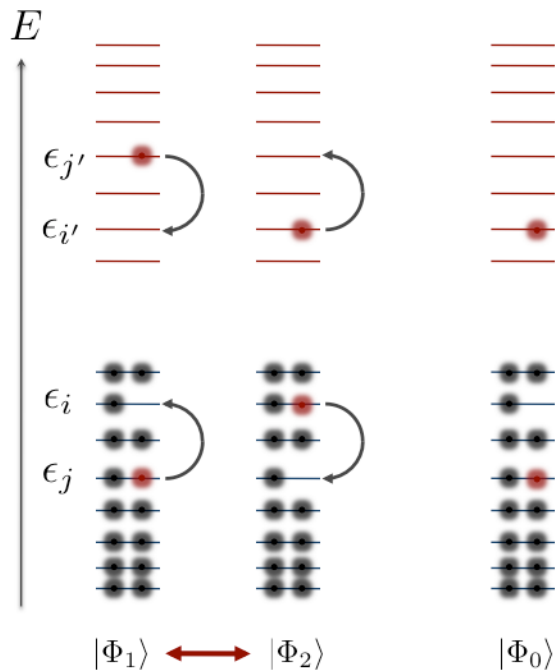
Figure 2. Scheme of the single-particle states and the dynamics involved during VIBRET. In the figure, the horizontal lines denote orbital levels of varying energy E and the circles denote electrons. The arrows indicate the joint electron exchange observed during VIBRET: the decay of an electron from a higher-energy conduction band orbital j' to a lower energy state i' leads to resonant excitation of an electron from an inner state in the valence band j to a higher energy state in the valence band i. Upon population inversion, the electron in the valence band i decays back into state j and resonantly excites the electron in level i' to level j'. Several of these cycles can be observed when the population exchange is energy conserving, i.e. when $\epsilon_i - \epsilon_j = \epsilon'_j - \epsilon'_i$. The complementary N-particle level structure and couplings are depicted in figure 3.

exchange in a generalized setting, and from a single-particle perspective, is shown in figure 2). The population from the higher energy conduction band orbital j' (in figure 1, $j' = \mathrm{LUMO}+1$) is transferred into the lower energy conduction band orbital i' ($i' = \mathrm{LUMO}$ in figure 1). Through the vibronic interactions, this decay resonantly drives an electron from the innermost valence orbital j ($j = \mathrm{HOMO}-1$ in figure 1) into the higher energy valence orbital i ($i = \mathrm{HOMO}$ in figure 1). Since the orbital energies are such that $\epsilon_{j'} - \epsilon_{i'} = \epsilon_i - \epsilon_j$, the process is energy conserving. In the case shown in figure 1(A), complete population transfer occurs in ~ 3 ps. At this stage, as shown in figure 2, the converse process occurs. Transfer of population from state i to the lower energy state j in the valence band resonantly excites the population from i' to j' in the conduction band. From the perspective of many-particle states, the system is effectively transferring population from state $|\Phi_1\rangle$ to state $|\Phi_2\rangle$, and vice versa. The computed vibronic evolution for the four-site chain (figure 1(A)) reveals at least six of these $|\Phi_1\rangle \to |\Phi_2\rangle \to |\Phi_1\rangle$ cycles before the population equilibrates.

    We have also observed this intriguing oscillatory population dynamics in 20-site chains (figure 1(B)). Here, the period of oscillation (~ 0.7 ps) is faster than in the $N = 4$ case and
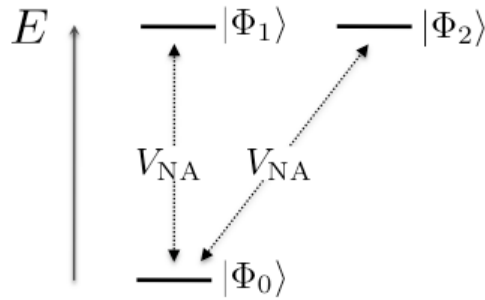
Figure 3. Level structure and couplings between N-particle electronic states able to sustain VIBRET. The vibronic dynamics couples the degenerate states $|\Phi_1\rangle$ and $|\Phi_2\rangle$ indirectly through a third auxiliary state $|\Phi_0\rangle$ via vibronic non-adiabatic coupling terms V_{NA} (see equation (8)) forming a Λ or V level system. Figure 2 depicts one possible single-particle electronic distribution for the states in the triad.

observable for 2–3 ps. That is, while the population dynamics is evident for $N = 20$, the process competes with population transfer into other electronic states that are coupled by the vibronic evolution. Such competition substantially decreases the lifetime of this population exchange with respect to the $N = 4$ example, where levels are spectrally isolated. In fact, for $N = 100$ (figure 1(C)) the electronic spectrum is so dense that the VIBRET is simply not observed.

3.1.2. Level structure and underlying couplings. A closer look at the three N-particle eigenstates of H_e involved in the dynamics, $|\Phi_0\rangle$, $|\Phi_1\rangle$ and $|\Phi_2\rangle$, reveals that they conform to the three-level system schematically shown in figure 3. Such a system consists of two degenerate orthonormal states, $|\Phi_1\rangle$ and $|\Phi_2\rangle$, with distinct electronic structure that are coupled indirectly through a third eigenstate $|\Phi_0\rangle$ via non-adiabatic coupling terms V_{NA}. The states $|\Phi_1\rangle$ and $|\Phi_2\rangle$ are uncoupled in the vibronic evolution and thus require the third 'auxiliary' state $|\Phi_0\rangle$ in order to transfer population between one another during the electron–vibrational dynamics. This resonant population transfer is a second-order process in V_{NA} that leaves the population of the auxiliary state approximately constant through the dynamics.

In order to understand how these effective couplings between levels $|\Phi_0\rangle$, $|\Phi_1\rangle$ and $|\Phi_2\rangle$ arise, consider the selection rules for non-adiabatic couplings in the context of (generic) mixed quantum-classical dynamics. For an electronic wavefunction $|\varphi(t)\rangle$ that satisfies equation (3) where the time dependence in $H_e(\boldsymbol{u})$ is assumed to arise from the fact that the nuclei satisfy some trajectory $\boldsymbol{u}(t)$, the coefficients in the expansion of $|\varphi(t)\rangle$ in terms of adiabatic eigenstates, i.e. $|\varphi(t)\rangle = \sum_k c_k(t)|\varphi_k[\boldsymbol{u}(t)]\rangle$ where $H_e(\boldsymbol{u})|\varphi_k[\boldsymbol{u}(t)]\rangle = E_k(t)|\varphi_k[\boldsymbol{u}(t)]\rangle$, satisfy [43]

$$i\hbar \frac{dc_i}{dt} = E_i(t)c_i - i\hbar \sum_k \langle\varphi_i|\frac{\partial}{\partial t}|\varphi_k\rangle c_k. \tag{7}$$

The second term is the non-adiabatic coupling V_{ik} between adiabatic states i and k and can be expressed as

$$V_{ik} = -i\hbar\dot{\boldsymbol{u}} \cdot \langle\varphi_i|\nabla_{\boldsymbol{u}}|\varphi_k\rangle = i\hbar\dot{\boldsymbol{u}} \cdot \frac{\langle\varphi_i|\nabla_{\boldsymbol{u}}H_e|\varphi_k\rangle}{E_i - E_k}. \tag{8}$$

Table 1. Electronic distribution and energy of all 19 possible states for an $N = 4$ PA chain. The distribution corresponds to the occupation of the four eigenorbitals in ascending energy. The electronic energy is given at the ground state optimal geometry ($u_1 = u_4 = 0$, $u_2 = 0.0847\,\text{Å}$, $u_3 = -u_1$). Note the degeneracies in the electronic spectra.

Distribution				E (eV)	Distribution				E (eV)
2	2	0	0	−11.95	1	1	0	2	1.81
2	1	1	0	−7.78	0	2	1	1	1.81
1	2	1	0	−5.97	0	2	0	2	3.61
2	1	0	1	−5.97	1	0	2	1	4.17
1	2	0	1	−4.17	1	0	1	2	5.97
2	0	2	0	−3.61	0	1	2	1	5.97
1	1	2	0	−1.81	0	1	1	2	7.78
2	0	1	1	−1.81	0	0	2	2	11.95
2	0	0	2	0.00					
1	1	1	1	0.00					
0	2	2	0	0.00					

Here we have taken into account the fact that the sole time dependence of the adiabatic states is through the nuclear coordinates such that $\frac{\partial}{\partial t}|\varphi_k\rangle = \dot{\boldsymbol{u}} \cdot \nabla_{\boldsymbol{u}}|\varphi_k\rangle$. In SSH chains, $V_{ik} \neq 0$ only if $\langle\varphi_i|\nabla_{\boldsymbol{u}} H_{\text{e}}|\varphi_k\rangle \neq 0$. This is the case even for degenerate states. Since H_{e} is a single-particle operator, it then follows that $V_{ik} \neq 0$ between states that differ by at most a single-particle transition. Two-particle transitions require terms in the Hamiltonian that are quartic in the creation and annihilation operators, which are absent from this model. More generally, for systems in which the electron–phonon coupling term in the Hamiltonian is quadratic in the creation and annihilation operators, in order for states to conform to figure 3 it suffices to guarantee that the selected states $|\Phi_1\rangle$ and $|\Phi_2\rangle$ are degenerate and differ by two-particle transitions, but that they are both a single-particle transition away from some state $|\Phi_0\rangle$. This holds even in the presence of electron–electron interactions as they do not contribute to the non-adiabatic transitions. The states employed in figure 1 satisfy precisely these requirements.

It is now natural to ask whether other triads that conform to the scheme in figure 3 will also display VIBRET. For illustrative purposes, we focus on the $N = 4$ example. In this case there are 19 possible electronic states and 5 possible degenerate manifolds (without taking into account spin degeneracies); they are tabulated in table 1. The states are labeled by the population of its four eigenorbitals, in ascending order. In this notation, the ground state would be state (2200), the first excited state (2110), etc. For instance, the superposition employed in figure 1(A) would correspond to (2101) + (2110). Figure 4 shows the orbital populations during the dynamics of chains initially prepared in the state of equation (4) with $b_0 = b_1$ and for different choices of $|\Phi_0\rangle$ and $|\Phi_1\rangle$. The two states involved in the superposition are indicated in each panel. The auxiliary state $|\Phi_0\rangle$ is further labeled by an 'a' after the orbital occupations. Figure 4(A) corresponds to a situation similar to that described in figure 1(A) and equation (5). The auxiliary state $|\Phi_0\rangle$ is the same but now the population, instead of being initially in state (2101), is initially allocated to the second state in the degenerate manifold (1210). A similar dynamics results, confirming the basic
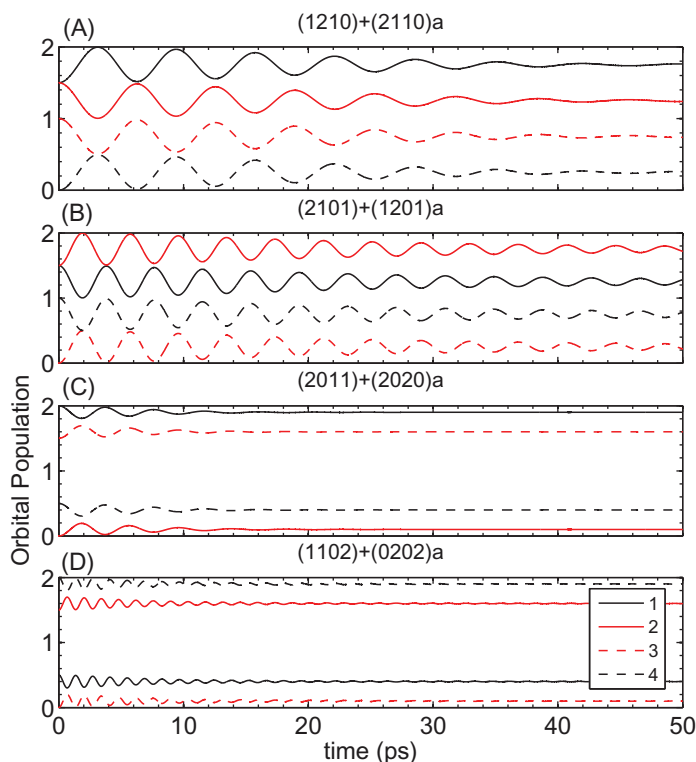
Figure 4. Different types of initial electronic superpositions $|\Omega\rangle = (1/\sqrt{2})(|\Phi_0\rangle + |\Phi_1\rangle) \otimes |\chi_0\rangle$ for $N = 4$ that exhibit VIBRET. The distribution of the states involved in each case are (A) $|\Phi_0\rangle = (2110)$, $|\Phi_1\rangle = (1210)$; (B) $|\Phi_0\rangle = (1201)$, $|\Phi_1\rangle = (2101)$; (C) $|\Phi_0\rangle = (2020)$, $|\Phi_1\rangle = (2011)$; (D) $|\Phi_0\rangle = (0202)$, $|\Phi_1\rangle = (1102)$. The energies of such states are shown in table 1. The numbers in the legend correspond to the eigenorbital labels in ascending energy.

identified level structure. The dynamics exemplified by figure 4(B) also uses the (2101)–(1210) degenerate manifold but here the auxiliary state $|\Phi_0\rangle$ is higher in energy, forming a Λ system instead of the V system explored in figure 1(A). Long-lived population transfer between $|\Phi_1\rangle$ and $|\Phi_2\rangle$ is also evident in this case but with a different timescale resulting from the change in the non-adiabatic coupling due to a change in $|\Phi_0\rangle$. Figures 4(C) and (D) demonstrate the effect in higher energy degenerate manifolds. In all the cases considered population transfer is as described in figures 2 and 3, and survives for tens of picoseconds. Naturally, if the system is prepared in a state that does not conform to the scheme in figure 3, no VIBRET will result. Supplementary figure S1 (available from stacks.iop.org/NJP/15/043004/mmedia) exemplifies such a situation for a system initially prepared in state (2200) + (2110).

Note that because the population exchange occurs between degenerate electronic states, there is no net absorption or emission of real phonons during the process. Hence, the limitations of Ehrenfest dynamics in describing the spontaneous emission of phonons [16] do not play a significant role here.

3.1.3. Dependence on the amplitudes of the initial superposition. Another significant aspect of the observed behavior is the dependence of the VIBRET on the amplitudes of the states involved
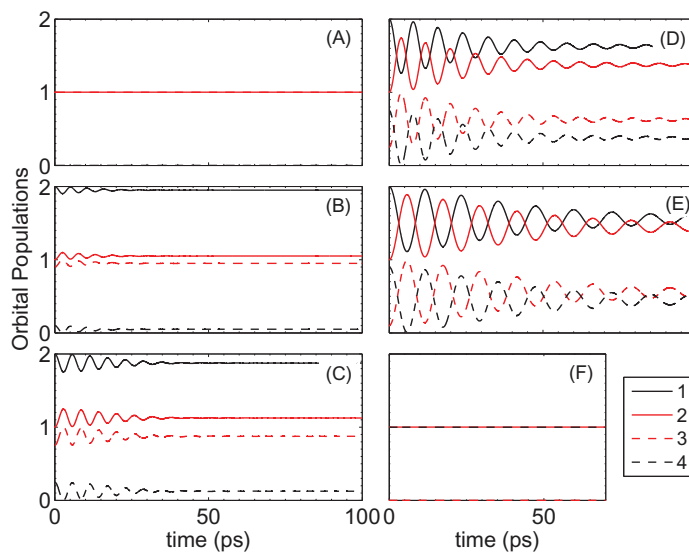
Figure 5. Dependence of the VIBRET on the amplitudes of the initial superposition. In this example, the initial state is given by $|\Omega\rangle = (b_0|\Phi_0\rangle + b_1|\Phi_1\rangle)|\chi_0\rangle$ with $b_0 = \sqrt{1 - |b_1|^2}$. Results are for $N = 4$ and for the superposition defined by the states in equation (5), i.e. $|\Phi_0\rangle = (2110)$ and $|\Phi_1\rangle = (2101)$. They correspond to (A) $|b_1|^2 = 0$; (B) $|b_1|^2 = 0.1$; (C) $|b_1|^2 = 0.25$; (D) $|b_1|^2 = 0.75$; (E) $|b_1|^2 = 0.9$; (F) $|b_1|^2 = 1$. The case of $|b_0|^2 = |b_1|^2 = 0.5$ is shown in figure 1(A). In all cases the initial coefficients where chosen to be real and positive. The numbers in the legend correspond to the eigenorbital labels in ascending energy.

in the superposition at the time of preparation. Figure 5 shows the orbital population dynamics for a chain with four sites initially prepared in the superposition defined by the states in equations (4) and (5) for different b_0 and b_1. When all the population is in the auxiliary state (i.e. $|b_0|^2 = 1$) no population transfer is observed (see figure 5(A)) because the vibrational degrees of freedom are not able to resonantly couple the auxiliary state $|\Phi_0\rangle$ with the degenerate manifold. As the population initially placed in the excited state manifold is increased (the progression shown in figures 5(B)–(F)), the amount of population exchanged during the dynamics changes. Because of the resonance structure in figure 3, only the population that is initially placed in the degenerate manifold can be exchanged, e.g. the state in which initially $|b_1|^2 = 0.9$ can exchange at most 0.9 electrons. In addition, by changing the initial coefficients in the superposition, one is changing the forces that act on the nuclei at $t = 0$ and thus, effectively, the strength of the non-adiabatic coupling terms during the evolution. This change in the strength of the non-adiabatic couplings modifies the timescale of the population oscillations and the lifetime of the process. Note that when all population is placed in the degenerate manifold (figure 5(F)), the strength of the non-adiabatic coupling terms is substantially reduced and no population exchange is observed in the simulated time window. We have observed this behavior in all of the cases considered and, as such, it is an inherent feature of this highly nonlinear vibronic evolution. In principle, the phenomenon does not require an initial superposition between states $|\Phi_0\rangle$ and $|\Phi_1\rangle$. In practice, however, such initial coherences introduce additional forces on the
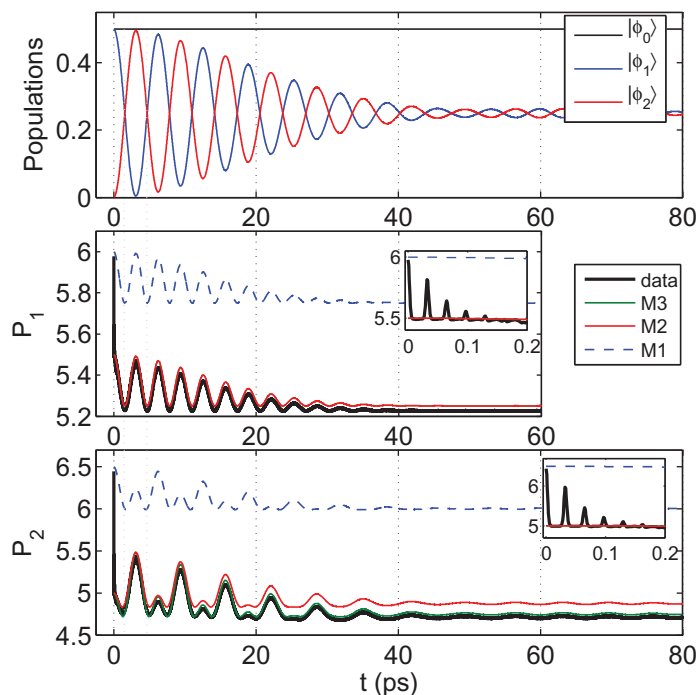
Figure 6. Electronic decoherence during VIBRET. The plot shows the populations of the many-body states $|\Phi_0\rangle$, $|\Phi_1\rangle$ and $|\Phi_2\rangle$ (top panel), the one-body purity (middle panel) and the two-body purity (bottom panel) for an $N = 4$ system initially prepared in the state defined by equations (4)–(6) with $b_0 = b_1$. The insets highlight the first 200 fs of evolution that are not resolved in the main plots. In the purity plots, the simulated data are shown in black. The colored lines represent a fully coherent (M1), partially coherent (M2) and completely incoherent (M3) model of the state of the system during the dynamics. In the middle panel the M2 and M3 lines are on top of one another and cannot be distinguished.

nuclei at initial time that enhance the effective non-adiabatic couplings, leading to a visible effect within the propagated time window.

3.2. Electronic coherence during the VIBRET

Consider now the electronic coherence properties of the VIBRET in order to determine whether the observed dynamics is coherent or incoherent. For definitiveness, we focus on the dynamics in figure 1(A) in which the system is initially prepared in the state defined by equations (4)–(6) with $N = 4$ and $b_0 = b_1$. The top panel of figure 6 shows the populations of the states $|\Phi_0\rangle$, $|\Phi_1\rangle$ and $|\Phi_2\rangle$, reconstructed from the orbital populations by supposing that only these three many-particle states participate in the dynamics. The plot clearly shows the population exchange between $|\Phi_1\rangle$ and $|\Phi_2\rangle$, and its decay, while the population of state $|\Phi_0\rangle$ remains approximately constant throughout.

The dynamics exemplified in the top panel of figure 6 (also figure 1(A)) strongly suggests the presence of a long-lived electronic coherence because they are reminiscent of beating

patterns resulting from superpositions between nearly degenerate states. If, in fact, the dynamics is a coherent process then the observed evolution would constitute a clear example of a long-lived coherence that is unquestionably electronic. That is, here, the observed beatings could arise from the effective coupling between states $|\Phi_1\rangle$ and $|\Phi_2\rangle$ that is introduced by the non-adiabatic coupling terms. The decay of the population exchange in the degenerate manifold would then suggest that a decoherence process is taking place with an unusually long decay constant (typical decoherence timescales obtained with this model of the vibronic evolution are of $\sim$10–100 fs [14]).

To examine this possibility, we now quantify the coherence properties during VIBRET. To proceed, it is useful to recall some basic facts about electronic decoherence in molecular systems. Electronic decoherence in molecules arises because of interactions with the nuclear degrees of freedom and can be understood in terms of nuclear dynamics on alternative electronic potential energy surfaces [11, 12, 24, 44]. To see this, consider the reduced electronic density matrix associated with a general entangled vibronic Born–Oppenheimer state of the form $|\Omega(t)\rangle = \sum_n e^{-iE_n t/\hbar}|\varphi_n\rangle|\chi_n(t)\rangle$,

$$\hat{\rho}_e(t) = \text{Tr}_N\{|\Omega(t)\rangle\langle\Omega(t)|\}$$
$$= \sum_{nm} e^{-i\omega_{nm}t}\langle\chi_m(t)|\chi_n(t)\rangle|\varphi_n\rangle\langle\varphi_m|. \tag{9}$$

Here the trace is over the nuclear states, $|\varphi_n\rangle$ are the electronic eigenstates $[H_{\text{elec}}|\varphi_n\rangle = E_n|\varphi_n\rangle]$, $|\chi_n(t)\rangle$ the nuclear wavepacket associated with each electronic level and $\omega_{nm} = (E_n - E_m)/\hbar$. Note that the magnitudes of the off-diagonal elements of $\hat{\rho}_e(t)$ are proportional to the nuclear overlaps $S_{nm}(t) = \langle\chi_m(t)|\chi_n(t)\rangle$. Hence, the loss of such $\hat{\rho}_e(t)$ coherences is a result of the evolution of the $S_{nm}(t)$ due to the vibronic dynamics. Standard measures of decoherence capture precisely this. For example, the purity of such an entangled vibronic state [45] is given by

$$\text{Tr}(\hat{\rho}_e^2(t)) = \sum_{nm} |\langle\chi_m(t)|\chi_n(t)\rangle|^2 \tag{10}$$

and decays with the overlaps of the nuclear wavepackets in the different electronic surfaces.

In order to quantify the coherences during VIBRET, one ideally would like to study the purity (equation (10)) directly. However, for many-electron systems, like the one considered here, the electronic density matrix $\hat{\rho}_e$ is a many-body quantity that is not easy to compute and hence reduced descriptions of the purity are required. Here we introduce and follow the dynamics of the one-body and two-body reduced purities, defined as

$$P_1(t) = \text{Tr}\{\hat{\rho}^2(t)\},$$
$$P_2(t) = \text{Tr}\{\hat{\Gamma}^2(t)\}, \tag{11}$$

where $\hat{\rho}$ and $\hat{\Gamma}$ refer to the one-body and two-body electronic density matrices. These quantities are defined as

$$\rho_p^q = \sum_{\sigma} \text{Tr}\{c_{p\sigma}^\dagger c_{q\sigma}\hat{\rho}_e\}, \tag{12}$$

$$\Gamma_{pq}^{sr} = \frac{1}{2}\sum_{\sigma,\sigma'} \text{Tr}\{c_{p\sigma}^\dagger c_{q\sigma'}^\dagger c_{r\sigma'} c_{s\sigma}\hat{\rho}_e\}. \tag{13}$$

Because the one-body purity is constructed from the one-body density matrix, it only informs us about coherences between states that differ at most by single-particle transitions. For example,

it cannot distinguish between a superposition and a mixture between states that differ by two (or more) particle transitions. Similarly, the two-body purity is only informative about the coherences between states that differ by at most two-particle transitions.

The middle and bottom panels of figure 6 show the dynamics of the reduced purities during VIBRET. In order to interpret the results, we consider three models of the state of the system that differ in the assumed degree of coherence. The models are defined by the following assumed forms for the electronic density matrix:

$$M1: \quad \hat{\rho}_e = (c_0|\Phi_0\rangle + c_1|\Phi_1\rangle + c_2|\Phi_2\rangle)(c_0^\star\langle\Phi_0| + c_1^\star\langle\Phi_1| + c_2^\star\langle\Phi_2|),$$

$$M2: \quad \hat{\rho}_e = |c_0|^2|\Phi_0\rangle\langle\Phi_0| + (c_1|\Phi_1\rangle + c_2|\Phi_2\rangle)(c_1^\star\langle\Phi_1| + c_2^\star\langle\Phi_2|), \quad (14)$$

$$M3: \quad \hat{\rho}_e = |c_0|^2|\Phi_0\rangle\langle\Phi_0| + |c_1|^2|\Phi_1\rangle\langle\Phi_1| + |c_2|^2|\Phi_2\rangle\langle\Phi_2|.$$

They represent, respectively, a fully coherent model (M1), a partially coherent model where only the coherences within the degenerate manifold are maintained (M2) and a fully incoherent model (M3). The purity resulting from the simulation is shown in black, while the colored lines show the purity expected for these three models, reconstructed by supposing that only the $|\Phi_0\rangle$, $|\Phi_1\rangle$ and $|\Phi_2\rangle$ many-particle states participate in the dynamics. The insets highlight the first 200 fs of evolution which are not resolved in the main plots.

From $P_1(t)$ (middle panel) we conclude that a fully coherent picture is not representative of the actual dynamics. Here, the system begins in a pure state and during the first 200 fs the system displays fast decoherence between the states in the initial $|\Phi_0\rangle$, $|\Phi_1\rangle$ superposition. The inset details this initial decoherence process. The recurrences observed in the one-body purity signal the vibrational dynamics in the excited state manifold [14] that lead to time dependence of the overlaps in equation (10). These recurrences are not captured by the models in equation (14) because they do not take into account the nuclear evolution. After this initial fast decoherence, P_1 oscillates, reflecting the population changes in the system throughout the dynamics. However, P_1 cannot distinguish between the partially coherent model M2 and the fully mixed case M3 because the coherence in M2 is between states that differ by two-particle transitions. In order to distinguish between these two cases, we follow the two-body purity $P_2(t)$ shown in the bottom panel. This quantity shows an initial fast decay (in $\sim$200 fs) due to the decoherence between states $|\Phi_0\rangle$ and $|\Phi_1\rangle$, followed by oscillations. After this initial fast decoherence dynamics, the model that best adjusts to the observed behavior is M3. That is, the observed population exchange, even when reminiscent of beatings in coherent superpositions, is really best described as a mixed state between $|\Phi_0\rangle$, $|\Phi_1\rangle$ and $|\Phi_2\rangle$. *We thus are forced to conclude that, contrary to intuition, after 200 fs the dynamics during VIBRET is a purely incoherent process.*

The dynamics is incoherent because superpositions between states $|\Phi_0\rangle$ and $|\Phi_1\rangle$ and $|\Phi_0\rangle$ and $|\Phi_2\rangle$ decohere quickly (of the order of $\sim$200 fs in the $N = 4$ case and of tens of fs for larger oligomers). Since all communication between $|\Phi_1\rangle$ and $|\Phi_2\rangle$ is then through $|\Phi_0\rangle$, a net incoherent process results. From a quantum-classical perspective, the V_{NA} in individual trajectories leads to coherences between the states. However, on average the V_{NA} leads to an incoherent coupling contributing to the incoherent dynamics. The observed directionality in the population exchange is due to the population imbalance between states $|\Phi_1\rangle$ and $|\Phi_2\rangle$. In fact, had we started with a state where $|\Phi_1\rangle$ and $|\Phi_2\rangle$ were equally populated, then no VIBRET would result.
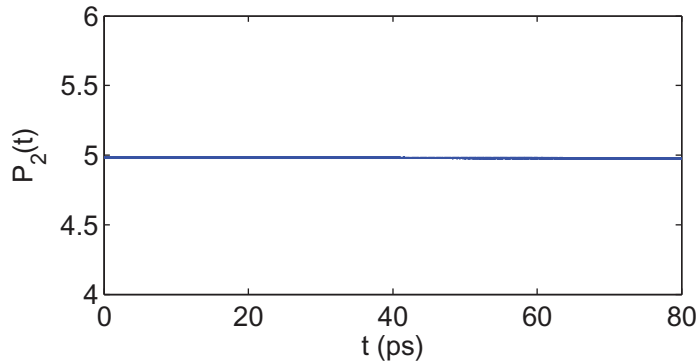
Figure 7. Two-body purity for an $N = 4$ chain prepared in state equation (15). The quantity $P_2(t)$ shows that this state starts and remains pure during the dynamics even when it is not a stationary state of the Hamiltonian.

3.3. What would constitute a superposition of electronic states that is truly robust to decoherence due to vibronic couplings?

Consider the dynamics where the same vibrational wavepacket is prepared in two degenerate electronic states, that is

$$|\Omega\rangle = \frac{1}{\sqrt{2}}(|\Phi_1\rangle + |\Phi_2\rangle) \otimes |\chi\rangle. \tag{15}$$

Figure 7 shows the time dependence of the two-body purity for an $N = 4$ system prepared in equation (15) with $|\Phi_1\rangle$ and $|\Phi_2\rangle$ defined by equations (5) and (6). For a coherent superposition one expects $P_2(t) \sim 5.0$ in this case, while a perfectly incoherent state would yield $P_2(t) = 4.5$. As can be seen, even when the initial state in equation (15) is not an equilibrium state of the vibronic Hamiltonian and leads to a complex electron–vibrational evolution, this initial superposition starts and remains pure throughout the dynamics. It constitutes a clear example of an electronic superposition state with coherence properties that are robust to the vibronic interactions of the chain.

   The feature that underlies these robust coherences is the fact that the superposition is between two electronic states with underlying potential energy surfaces that differ at most by a constant factor. In this case, the states $|\Phi_1\rangle$ and $|\Phi_2\rangle$ are degenerate in all conformational space, i.e. $E_1(\boldsymbol{u}) = E_2(\boldsymbol{u})$ for all $\boldsymbol{u}$, where $E_i(\boldsymbol{u})$ is the potential energy surface associated with adiabatic state i. Consequently, a given vibrational wavepacket $|\chi\rangle$ will move identically on both surfaces and the nuclear overlap $S_{12}(t) = \langle\chi_1(t)|\chi_2(t)\rangle$ that determines the electronic coherence between the two states (recall equation (9)) is unaffected by the dynamics. In other words, the two levels involved couple to the environmental bath identically, preventing the bath from entangling with (and thus inducing decoherence of) the system. This is the case provided that the two states are spectrally isolated from other electronic states.

   The quantum structure involved in these robust coherences falls into the class of decoherence-free subspaces [46, 47]. Such a subspace has been suggested (see e.g. [48]) to underlie the long coherences in the photosynthetic example, although approximate explicit computations [49] have not yet revealed such a structure. By contrast, the triad in figure 3 does not conform to a decoherence-free subspace because the potential energy surface of the third electronic state $|\Phi_0\rangle$ generally differs by more than a constant to that of the degenerate states.

4. Conclusions

We have identified a new basic feature of the vibronic evolution of a molecular system that we term VIBRET. In this process, via the vibronic interactions, the decay of an electron in the conduction band to a lower energy state resonantly excites an electron in the valence band, and vice versa. In PA oligomers (as described by the SSH Hamiltonian in a mixed quantum-classical approximation), the population transfer can survive for up to tens of picoseconds and observe several cycles of population exchange. The process requires two degenerate electronic states with distinct electronic configurations that are indirectly coupled to a third state via vibronic interactions. For Hamiltonians with electron–phonon coupling terms that are at most quadratic in the fermionic operators, such population exchange is realized between degenerate states that differ by two-particle transitions but that are both a single-particle transition away from a third auxiliary state.

The observed population dynamics is strongly suggestive of an electronic coherent process with an unusually long decoherence time. However, things are not always what they seem and, contrary to intuition, an analysis of the one-body and two-body electronic purities shows that VIBRET occurs incoherently.

We have also demonstrated electronic superpositions in a molecular system that is robust to decoherence induced by vibronic couplings. As shown, robust electronic superpositions can arise when the underlying potential energy surfaces of the states involved in the superposition differ by a constant factor. Under such conditions the vibronic evolution of an initially separable state does not lead to entanglement between the electronic and vibrational degrees of freedom and thus does not lead to decoherence.

We expect the phenomena described here to be of importance in understanding vibronic and coherence phenomena in molecules, macromolecules and bulk materials. Future prospects include performing fully quantum simulations of VIBRET and determining ways to manipulate the identified robust electronic coherences.

Acknowledgments

References

[1] Köuppel H, Domcke W and Cederbaum L S 1984 *Adv. Chem. Phys.* **57** 59
[2] Frank-Kamenetskii M D and Lukashin A V 1975 *Sov. Phys.—Usp.* **18** 391
[3] Adachi S, Kobryanskii V M and Kobayashi T 2002 *Phys. Rev. Lett.* **89** 027401
[4] Polli D *et al* 2010 *Nature* **467** 440
[5] Levine B G and Martínez T J 2007 *Annu. Rev. Phys. Chem.* **58** 613
[6] Christopher P, Shapiro M and Brumer P 2006 *J. Chem. Phys.* **125** 124310

IOP Institute of Physics ⦿ DEUTSCHE PHYSIKALISCHE GESELLSCHAFT

[7] Grinev T, Shapiro M and Brumer P 2013 *J. Chem. Phys.* **138** 044306
[8] Link S and El-Sayed M A 1999 *J. Phys. Chem.* B **103** 8410
[9] Hildner R, Brinks D and van Hulst N F 2011 *Nature Phys.* **7** 172
[10] Prezhdo O V and Rossky P J 1997 *J. Chem. Phys.* **107** 5863
[11] Hwang H and Rossky P J 2004 *J. Phys. Chem.* B **108** 6723
[12] Franco I, Shapiro M and Brumer P 2008 *J. Chem. Phys.* **128** 244905
[13] Subotnik J E and Shenvi N 2011 *J. Chem. Phys.* **134** 244114
[14] Franco I and Brumer P 2012 *J. Chem. Phys.* **136** 144501
[15] Heeger A J, Kivelson S, Schrieffer J R and Su W P 1988 *Rev. Mod. Phys.* **60** 781
[16] Stella L, Miranda R P, Horsfield A P and Fisher A J 2011 *J. Chem. Phys.* **134** 194105
[17] Ness H and Fisher A J 1999 *Phys. Rev. Lett.* **83** 452
[18] Teramoto T, Wang Z, Kobryanskii V M, Taneichi T and Kobayashi T 2009 *Phys. Rev.* B **79** 033202
[19] Tretiak S, Saxena A, Martin R L and Bishop A R 2003 *Proc. Natl Acad. Sci. USA* **100** 2185
[20] Tully J C 1998 *Faraday Discuss.* **110** 407
[21] Streitwolf H W 1998 *Phys. Rev.* B **58** 14356
[22] Johansson A and Stafström S 2002 *Phys. Rev.* B **65** 045207
[23] Hillery M, O'Connell R F, Scully M O and Wigner E P 1984 *Phys. Rep.* **106** 121
[24] Kamisaka H, Kilina S V, Yamashita K and Prezhdo O V 2006 *Nano Lett.* **6** 2295
[25] Engel G S, Calhoun T R, Read E L, Ahn T-K, Mancal T, Cheng Y-C, Blankenship R E and Fleming G R 2007 *Nature* **446** 782
[26] Collini E, Wong C Y, Wilk K E, Curmi P M G, Brumer P and Scholes G D 2010 *Nature* **463** 644
[27] Panitchayangkoon G, Hayes D, Fransted K A, Caram J R, Harel E, Wen J, Blankenship R E and Engel G S 2010 *Proc. Natl Acad. Sci. USA* **107** 12766
[28] Collini E and Scholes G D 2009 *Science* **323** 369
[29] Lee H, Cheng Y-C and Fleming G R 2007 *Science* **316** 1462
[30] Mohseni M, Rebentrost P, Lloyd S and Aspuru-Guzik A 2008 *J. Chem. Phys.* **129** 174106
[31] Lloyd S 2009 *Nature Phys.* **5** 164
[32] Cheng Y-C and Fleming G R 2009 *Annu. Rev. Phys. Chem.* **60** 241
[33] Ishizaki A and Fleming G R 2009 *Proc. Natl Acad. Sci. USA* **106** 17255
[34] Renaud N, Ratner M A and Mujica V 2011 *J. Chem. Phys.* **135** 075102
[35] Huo P and Coker D 2011 *J. Phys. Chem. Lett.* **2** 825
[36] Kelly A and Rhee Y M 2011 *J. Phys. Chem. Lett.* **2** 808
[37] Pachon L A and Brumer P 2011 *J. Phys. Chem. Lett.* **2** 2728
[38] Pachon L A and Brumer P 2012 *Phys. Chem. Chem. Phys.* **14** 10094
[39] Strümpfer J, Sener M and Schulten K 2012 *J. Phys. Chem. Lett.* **3** 536
[40] Ishizaki A and Fleming G R 2012 *Annu. Rev. Condens. Matter Phys.* **3** 333
[41] Brumer P and Shapiro M 2012 *Proc. Natl Acad. Sci. USA* **109** 19575
[42] Pachon L A and Brumer P 2013 *Phys. Rev.* A **87** 022106
[43] Tully J C 1990 *J. Chem. Phys.* **93** 1061
[44] Habenicht B F, Kamisaka H, Yamashita K and Prezhdo O V 2007 *Nano Lett.* **7** 3260
[45] Jiang X-P and Brumer P 1993 *Chem. Phys. Lett.* **208** 179
[46] Lidar D A, Chuang I L and Whaley K B 1998 *Phys. Rev. Lett.* **81** 2594
[47] Kwiat P G, Berglund A J, Altepeter J B and White A G 2000 *Science* **290** 498
[48] Abramavicius D and Mukamel S 2011 *J. Chem. Phys.* **134** 174504
[49] Shim S, Rebentrost P, Valleau S and Aspuru-Guzik A 2012 *Biophys. J.* **102** 649